RAPID COMMUNICATIONS

PHYSICAL REVIEW C VOLUME 47, NUMBER 5 MAY 1993

Exotic nuclei in a relativistic mean-field approach

J. A. Sheikh
Tata Institute of Fundamental Research, Bombay 400 005, India

P. Ring
Physik-Department der Technischen Universität München, D-8046 Garching, Federal Republic of Germany
(Received 14 September 1992)

The neutron rich Zr isotopes are studied in a relativistic mean-field approach. A transition from spherical to strongly deformed shapes is obtained around $A \simeq 100$ and ground state deformations are found, which are in size close to superdeformed shapes. Furthermore, very large radii are predicted in the vicinity of the neutron drip line due to the combined effects of deformation and neutron excess.

PACS number(s): 27.70.+j, 21.10.Hw, 21.60.Ev, 21.60.Jz

The nuclei far from the β-stability line which are referred to as exotic nuclei have attracted considerable interest in recent years [1]. Undoubtedly the study of these exotic nuclei is destined to be one of the frontier fields in nuclear structure physics. The recent experiments [2–5] with radioactive beams have opened up this new era in nuclear spectroscopy. From the analysis of the interaction cross sections in these radioactive beam experiments it has been possible to determine the sizes of the neutron drip line nuclei, e.g., ^{11}Li, ^{14}Be, and ^{17}B. It is observed that these nuclei have very large root mean square (rms) radii. In the case of ^{11}Li the large radius has been attributed to the weak binding of the dineutron to the ^{9}Li core. This weak binding leads to the formation of a halo [6] around the ^{9}Li core that extends to several times the nuclear radius and consequently to a large matter radius for ^{11}Li.

In the heavier (above p-shell) nuclei both proton and neutron drip lines appear to be out of reach with the exception of the $A \simeq 100$ region. The spectroscopic studies in this $A \simeq 100$ region have become possible by observing [7] prompt $\gamma\gamma$ coincidences in fisson fragments (f) following the heavy-ion fusion reactions ^{232}Th(^{18}O,f) and ^{238}U(Li,f). This region is interesting from the standpoint that these nuclei are expected to be strongly deformed. The question that we would like to address in the present study is: What are the deformation effects for the neutron skin thickness? (The neutron skin thickness is the distance between the locations of the surfaces of the neutron and proton density distributions.) Recently it has been shown [8] in the Thomas-Fermi approach that this neutron skin thickness grows quite rapidly in the vicinity of the neutron drip line.

Theoretically $A \simeq 100$ nuclei have been partially studied in the Nilsson-Struntinsky (NS) [9–11] and in the density dependent Hartree-Fock (DDHF) [12, 13] formalism. It is apparent from the NS calculations that the results are very sensitive to the parameters (κ, μ) for the spin orbit and the l^2 term in the single particle potential [11]. For the density dependent HF calculations it is to be noted here that in order to have reliable predictions for the neutron rich nuclei an interaction with good isospin asymmetry property is needed. Some of the versions of the DDHF approach, for example with Skyrme-II interaction [14], do not satisfy this requirement.

In the present work we employ the relativistic mean-field (RMF) approach. In this RMF theory the aforementioned drawbacks in the NS and in the DDHF approach are remedied in a natural way. The proper spin-orbit coupling is guaranteed by the Dirac equation for the baryon fields through a careful adjustment of fields for scalar (σ) and vector (ω) mesons. The isospin asymmetry is generated by the isovector ρ-meson coupling term in the Lagrangian density so that the ρ-meson contribution (E_ρ) becomes increasingly important for large isospin asymmetry. Moreover, recently it has been shown in a detailed study [15], that the RMF approach gives a very good description of the ground state properties of finite nuclei throughout the mass table.

We start with the Lagrangian density [15, 16]

$$\begin{aligned}\mathcal{L} = {} & \bar{\psi}\left(\imath\gamma^\mu\partial_\mu - M\right)\psi + \frac{1}{2}\partial^\mu\sigma\partial_\mu\sigma - U(\sigma) - g_\sigma\bar{\psi}\psi\sigma \\ & -\frac{1}{4}\Omega^{\mu\nu}\Omega_{\mu\nu} + \frac{1}{2}m_\omega^2\omega^\mu\omega_\mu - g_\omega\bar{\psi}\gamma^\mu\psi\omega_\mu \\ & -\frac{1}{4}\mathbf{R}^{\mu\nu}\mathbf{R}_{\mu\nu} + \frac{1}{2}m_\rho^2\boldsymbol{\rho}^\mu\boldsymbol{\rho}_\mu - g_\rho\bar{\psi}\gamma^\mu\boldsymbol{\tau}\psi\boldsymbol{\rho}_\mu \\ & -\frac{1}{4}F^{\mu\nu}F_{\mu\nu} - e\bar{\psi}\gamma^\mu\frac{(1-\tau_3)}{2}\psi A_\mu, \end{aligned} \tag{1}$$

the sigma (σ) meson is assumed to move in a nonlinear potential [17]

$$U(\sigma) = \frac{1}{2}m_\sigma\sigma^2 + \frac{1}{3}g_2\sigma^3 + \frac{1}{4}g_3\sigma^4, \tag{2}$$

M, m_σ, m_ω, and m_ρ are the nucleon-, σ-, ω-, and ρ-meson masses, respectively. g_σ, g_ω, g_ρ and $\frac{e^2}{4\pi} = \frac{1}{137}$ are the coupling constants for the σ-, ω-, ρ-meson and for the photon. The $\Omega^{\mu\nu}$, $\mathbf{R}^{\mu\nu}$, and $F^{\mu\nu}$ are the field tensors for the vector mesons and the photons.

For the eight parameters m_σ, m_ω, m_ρ, g_σ, g_ω, g_ρ, g_2, and g_3 we used the set NL1 [15] which has been adjusted in Ref. [18] to properties of nuclear matter and of finite nuclei. The classical equations of motion derived from the Lagrangian Eq. (1) are solved by expansion of the Dirac spinors and the meson fields in a cylindrical oscillator basis with $N_F = 12$ major shells. Details of this technique are described in Ref. [15]. Results for selected

TABLE I. Results of the relativistic mean-field (RMF) calculations for Zr isotopes: binding energies per particle E/A (in MeV), root mean square radii (rms) for neutrons (protons) r_n (r_p), charge (r_c) radii (in fm), proton (neutron) quadrupole moments Q_n (Q_p) (in b) and hexadecupole moments H_n (H_p) (in b^2). $N_F = 12$ major oscillator shells have been used with the oscillator parameter $\hbar\omega_0 = 41A^{1/3}$ and the deformation parameters of the basis $\beta_0 = 0.0$ ($A \leq 100$), 0.41 ($A = 100$), 0.55 ($A \geq 102$). The results are found to be stable with respect to small changes of these basis parameters and with respect to a change from $N_F = 12$ to $N_F = 13$. The experimental data are taken from Ref. [20] (E/A), Ref. [22] (quadrupole moments), and Ref. [23] (charge radii).

A		E/A	r_n	r_p	r_c	Q_n	Q_p	H_n	H_p
84	RMF	-8.58	4.23	4.22	4.23	0.00	0.00	0.00	0.00
	SkIII		4.20	4.22		0.00	0.00		
	Expt.	-8.55					2.09		
90	RMF	-8.73	4.36	4.21	4.29	0.00	0.00	0.00	0.00
	SkIII	-8.72	4.30	4.25		0.00	0.00		
	Expt.	-8.71			4.27		0.80		
94	RMF	-8.64	4.47	4.23	4.32	0.00	0.00	0.00	0.00
	SkIII	-8.62	4.40	4.31		1.99	1.40		
	Expt.	-8.67			4.33		0.81		
96	RMF	-8.59	4.53	4.24	4.32	0.00	0.00	0.00	0.00
	SkIII	-8.57	4.46	4.36		3.0	2.10		
	Expt.	-8.63			4.40		0.74		
98	RMF	-8.53	4.60	4.27	4.34	0.00	0.00	0.00	0.00
	SkIII	-8.53	4.53	4.42		4.62	3.20		
	Expt.	-8.58							
100	RMF	-8.48	4.75	4.44	4.63	6.48	4.15	0.26	0.15
	SkIII	-8.49	4.61	4.47		6.00	3.97		
	Expt.	-8.52					3.01		
106	RMF1	-8.27	4.90	4.48	4.75	6.93	4.02	0.18	0.12
	RMF2	-8.28	4.91	4.48	4.75	6.84	3.93	0.20	0.12
110	RMF1	-8.10	5.02	4.54	4.85	8.06	4.31	0.22	0.12
	RMF2	-8.11	5.02	4.53	4.84	7.52	4.04	0.21	0.11

Zr isotopes ranging from $A = 84$ to $A = 110$ are presented in Table I. Pairing correlations are taken into account in the constant gap approximation [19]. The gap parameters have been fixed from the measured odd-even mass differences [20]. The masses of the Zr isotopes are known up to $A = 102$. For $A = 104$ to 110, two sets of calculations have been performed. In the first denoted by RMF1 in Table I, the pair gaps $\Delta_p = 1.78$ MeV and $\Delta_n = 1.145$ MeV have been employed. These pair gaps correspond to ^{102}Zr. In order to test the sensitivity of the results with respect to these values, the calculations have been repeated (and denoted by RMF2 in Table I) with a second set of slightly different pair gaps $\Delta_p = 2.0$ MeV and $\Delta_n = 1.5$ MeV. As is evident from the comparison of the two columns RMF1 and RMF2, the calculations appear to be reasonably independent of these moderate readjustments in the pair gaps.

It is clear from the third column of Table I that the binding energies per particle (E/A) are reproduced to a few tenths of a percent of the measured masses. The binding energy increases until $A = 90$ and then it drops as expected since ^{90}Zr is the closed shell nucleus. In Table II we show the different contributions to the binding energy, the sum of the single particle energies $E_{\rm part}$, the various linear contributions of the meson fields (E_σ, E_ω, and E_ρ), of the nonlinear terms in the σ field ($E_{\sigma_{\rm NL}}$) and of the Coulomb field E_C, the pairing energy $E_{\rm pair}$ and the center of mass correction $E_{\rm c.m.}$. We observe a considerable cancellation between the attractive σ field and the repulsive vector fields and an increasing importance of the ρ field with increasing neutron excess.

The neutron (Q_n) and proton (Q_p) quadrupole moments in Table I vanish (spherical shape) until $A = 98$. But between $A = 98$ and $A = 100$ we observe a sharp transition to deformed shapes with $Q_n = 6.48$ and $Q_p = 4.15$ b. Experimental data show a similar transition from rather small quadrupole moments below $A = 98$ to a large value of $Q = 3.01$ b for $A = 100$, which is somewhat smaller than our value. We have to keep in mind, however, that mean-field theory does not take into account fluctuations, which play an important role in the

TABLE II. The various contributions to the total energy E.

	^{90}Zr	^{100}Zr	^{110}Zr
$E_{\rm part}$	-2249.15	-2465.19	-2612.87
E_σ	12 674.56	13 783.67	14 598.93
$E_{\sigma_{\rm NL}}$	-225.59	-258.28	-294.91
E_ω	-10 693.74	-11 589.99	-12 225.26
E_ρ	-14.33	-45.79	-88.51
E_C	-256.61	-247.96	-242.35
$E_{\rm pair}$	-13.96	-17.80	-19.32
$E_{\rm c.m.}$	-6.86	-6.63	-6.42
E	-785.69	-847.98	-890.74
E/A	-8.730	-8.480	-8.098

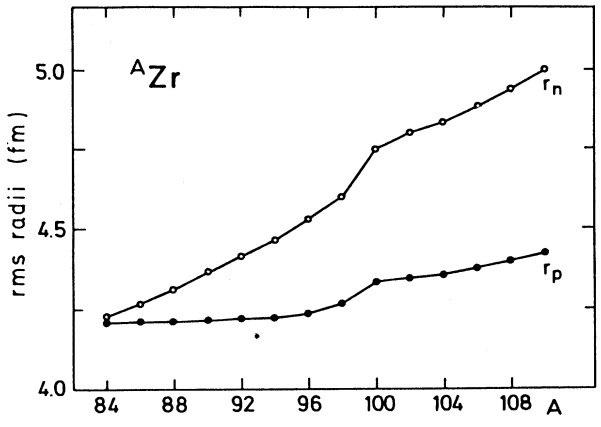

FIG. 1. Neutron and proton root mean square radii r_n (r_p) for all the studied Zr isotopes from $A = 84$ to 110. The sudden rise in r_p about $A = 98$ is due to the shape transition from spherical to strongly deformed. The neutron radii are observed to be increasing steadily with the neutron excess.

vicinity of phase transitions. Earlier DDHF calculations [13] with the force Skyrme III show a similar transition somewhat earlier between $A = 96$ and $A = 98$. They also give the relatively large value of $Q = 3.75$ b for $A = 100$.

Beyond the shape transition the deformation is seen to saturate. If one applies the relation $Q = (5/16\pi)^{1/2}3/(4\pi)AR^2\beta$, the quadrupole moment of $A = 100$ corresponds to $\beta \simeq 0.45$. This deformation β value is quite large and may be regarded as close to that of a superdeformed shape. Recent experiments of the Daresbury group [21] found that the nucleus ^{102}Zr is strongly prolate deformed with a deformation parameter $\beta = 0.43$, which is in excellent agreement with our results. More interestingly the asymmetry between the neutron and proton deformations is in our calculations observed to increase with neutron excess. The neutron quadrupole moment at the neutron drip line ($A = 110$) is almost twice the corresponding proton quadrupole moment. This is expected to give rise to a strong collective $M1$ mode.

Analyzing the details of this change in shape between $A = 98$ and $A = 100$ in our calculations we find a reoccupation of the levels in the vicinity of the Fermi level. The two additional neutrons are built into the deformation driving $1h_{11/2}$ shell with the major quantum number $N = 5$. This causes a polarization of the core and a move of roughly two pairs of particles from the $N = 3$ to the $N = 4$ shell for both protons and neutrons, i.e., a transition to a deformed shape.

The neutron and proton rms radii are plotted in Fig. 1. The proton rms radius r_p is constant until $A = 98$. It increases between $A = 98$ and $A = 100$ and stays almost stagnant beyond this point. The increase of r_p around $A = 98$ is clearly due to the phase transition from spherical to strongly deformed shape where two protons are moved from the $N = 3$ to the $N = 4$ shell, which has a larger radius. The neutron radius r_n shows a similar step at the transition point, but apart from that it increases steadily with the mass number because of the growing neutron excess. It reflects the fact that more and more neutrons are built into the shells with $N = 4$ and $N = 5$. At the shape transition one pair is moved from the $N = 3$ to the $N = 4$ shell. This is a polarization effect, which we call the reinforcing effect of deformation and neutron excess. In the vicinity of the neutron drip line the difference in the two rms radii is approximately 0.48 fm.

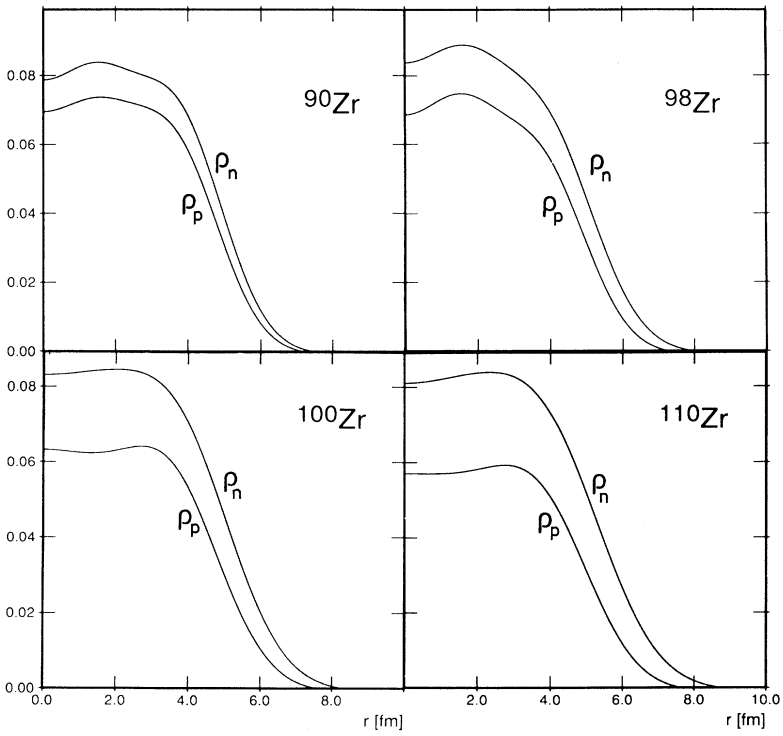

FIG. 2. The L=0 component of baryon point densities for protons (ρ_p) and neutrons (ρ_n) for the nuclei ^{90}Zr, ^{98}Zr, ^{100}Zr, and ^{110}Zr isotopes. A very large neutron skin thickness obtained for ^{110}Zr.

This neutronization of the nuclear surface will be more transparent in a plot of the proton and neutron density distributions.

The $L = 0$ component of the projected deformed baryon density [15] is the spherical symmetrical density of the ground state with angular momentum 0 in the laboratory frame. In Fig. 2 we show the contributions of protons and neutrons to this density for the nuclei ^{90}Zr, ^{98}Zr, ^{100}Zr, and ^{110}Zr. In the case of ^{90}Zr the proton (neutron) density distributions ρ_p^0 (ρ_n^0) show minor deviations in the nuclear interior and at the surface the two distributions are very similar. The calculated value for r_n in this nucleus is in agreement with the experimental value shown in Table I within the error bars. Between $A = 90$ and $A = 98$ the proton density changes only very little; the neutron density increases somewhat in the interior and considerably in the surface region. The shape transition between $A = 98$ and $A = 100$ is connected with a shift of proton density from the center to the surface reflecting the movement of particles from the $N = 3$ to the $N = 4$ shell. Afterwards the proton density changes very little. With the increasing neutron excess above $A = 100$, the additional neutrons are built mostly into the surface and the neutron skin thickness grows very rapidly and has quite a large value in the vicinity of the neutron drip line ($A = 110$). The scalar densities depict a very similar behavior.

From the present study of the relativistic mean-field calculations for the Zr isotopes it is possible to draw the following inferences: (i) A shape transition from spherical to strongly deformed is obtained around $A = 100$ and it is predicted that it may be possible to observe deformations close to those of superdeformed nuclei in the ground state. The possible candidates are ^{100}Zr, ^{102}Zr, and ^{104}Zr. (ii) The neutron radii are seen to increase steadily with neutron excess and a very large neutron skin thickness is obtained close to the neutron drip line. The probable consequences of this large neutron skin thickness on the measurable quantities are presently being pursued.

The authors would like to express their gratitude to D.M. Brink, R.R. Hilton, W. Koepf, M.A. Nagarajan, M.K. Pal, Dipti Pal, J.O. Rasmussen, and D.D. Warner for a number of useful discussions. This work was supported in part by Bundesministerium für Forschung und Technologie under Project No. 06 MT-733.

[1] P.G. Hansen, Phys. Scr. **T32**, 21 (1990).
[2] I. Tanihata *et al.*, Phys. Rev. Lett. **55**, 2676 (1985).
[3] I. Tanihata *et al.*, Phys. Lett. B **206**, 592 (1988).
[4] I. Tanihata, Nucl. Phys. **A488**, 113 (1988).
[5] E. Liatard *et al.*, Europhys. Lett. **13**, 401 (1990).
[6] P.G. Hansen and B. Johnson, Europhys. Lett. **4**, 409 (1987).
[7] Y. Abdelraham *et al.*, Daresbury Laboratory Annual Report, 1988/1989, page 11.
[8] W.D. Myers, in Proceedings of the First International Conference on Radioactive Nuclear Beam, Berkely, CA, 1989, edited by J.M. Nitschke (unpublished), p. 269.
[9] P. Möller and J.R. Nix, At. Data Tables **26**, 165 (1981).
[10] S. Aberg, Phys. Scr. **25**, 23 (1982).
[11] K. Hyde, J. Moreau, and M. Waroquier, Phys. Rev. C **29**, 1859 (1984).
[12] U. Mosel, P.-G. Zint, and K.H. Passler, Nucl. Phys. **A236**, 252 (1974).
[13] P. Bonche *et al.*, Nucl. Phys. **A443**, 39 (1985).
[14] M. Beiner *et al.*, Nucl. Phys. **A238**, 29 (1975).
[15] Y.K. Gambhir, P. Ring, and A. Thimet, Ann. Phys. (N.Y.) **198**, 132 (1990).
[16] B.D. Serot and J.D. Walecka, Adv. Nucl. Phys. **198**, 1 (1986).
[17] J. Boguta and A.R. Bodmer, Nucl. Phys. **A292**, 413 (1977).
[18] P.G. Reinhard, M. Rufa, J. Maruhn, W. Greiner, and J. Friedrich, Z. Phys. A **323**, 13 (1986).
[19] P. Ring and P. Schuck, *The Nuclear Many-Body Problem* (Springer-Verlag, New York, 1980).
[20] A. H. Wapstra and G. Audi, Nucl. Phys. **A432**, 1 (1985).
[21] Y. Abdelrahman *et al.*, Daresbury Laboratory, Annual Report, 1990.
[22] S. Raman, C.H. Malarkey, W.T. Milner, C.W. Nester, and P.H. Stelson, At. Data Nucl. Data Tables **36**, 1 (1987).
[23] H. de Vries, C.W. de Jager, and C. de Vries, At. Data Nucl. Data Tables **36**, 495 (1987).